Catalysis Science & Technology

Accepted Manuscript

ROYAL SOCIETY OF CHEMISTRY

www.rsc.org/catalysis

Effects of Preparation Variables on an Alumina-Supported FeCuK Fischer-Tropsch Catalyst

Kamyar Keyvanloo,[a] Jonathon B. Horton,[a] William C. Hecker,[a] Morris D. Argyle[a,]*

[a]Chemical Engineering Department, Brigham Young University, 350 CB, Provo, UT 84602, USA

**Corresponding author: mdargyle@byu.edu; telephone: 1-801-422-6239*

Abstract

This paper investigates the effects of various, carefully-chosen preparation methods on the performance of Fischer-Tropsch (FT) alumina-supported iron/copper/potassium ($FeCuK/Al_2O_3$) catalysts. Two tested preparation methods (co-impregnation and non-aqueous slurry impregnation) yielded supported Fe catalysts with better catalyst performance than previously thought possible. These two supported iron catalysts have high reaction rates (114–154 mmol $(CO+H_2)/g_{cat}/MPa/h$), good productivity (0.26–0.29 $g_{HC}/g_{cat}/h$), and reasonable stability. In fact, both catalysts are more active than any supported Fe catalyst reported outside our group and compare favorably with unsupported catalysts. Superior activity, coupled with the high strength of a supported catalyst, make these catalysts excellent candidates for use in slurry bubble column reactor (SBCR) applications.

Keywords: Fischer-Tropsch, Supported iron catalyst, Preparation variables, High activity

1. Introduction

Cobalt (Co) catalysts have been the subject of far more Fischer-Tropsch Synthesis (FTS) research than iron (Fe) catalysts due to their longevity and favorable reaction rates. However, commercial Fe has advantages over Co including lower cost, lower methane selectivity, and high water-gas shift activity. Commercial Fe catalysts produced for FTS are unsupported. Therefore, very little work on supported Fe catalysts is reported in the literature.[1-3]

Since the 1950's, the South African company Sasol has been one of the few in industry to prefer Fe catalysts.[4] Sasol has worked mostly with $Fe/Cu/K/SiO_2$ as an unsupported Fe catalyst. Bukur et al.[5] reported a weight-time yield of 450 mmol $(CO+H_2)/g_{Fe}/h/MPa$ and a C_{2+} hydrocarbon productivity of 0.86 $g_{HC}/g_{Fe}/h$ for $100Fe/3Cu/4K/16SiO_2$ at 260 °C and 2.2 MPa. Despite their high activity and favorable selectivity, unsupported Fe catalysts are generally too weak mechanically to be used in slurry bubble column reactors (SBCR's), which are the most thermally efficient and economical reactors.[6] Unfortunately, the severe conditions inside SBCR's grind weaker catalysts into fine

powders, resulting in excessive catalyst loss and plugging in the catalyst recovery system. These fine powders also render catalyst separation from the product nearly impossible. The US Department of Energy (DOE) performed a demonstration with a precipitated catalyst in a SBCR and found that attrition of the catalyst quickly plugged the filtering system, which required the reactor to be shut down within 24 h of startup.[6] O'Brien et al.[2] also concluded that supported Fe catalysts are far more attrition resistant than unsupported catalysts. They reported that unsupported precipitated catalysts, even with spray drying prior to calcination, were abraded from an initial particle size distribution of 30–50 µm down to 1–3 µm in just 24 h.

Among supported FT catalysts, the prevalent reasons for preferring Co catalysts over Fe are the inferior rates and selectivities of supported Fe catalysts.[7] Strong metal-support interaction is thought to cause lower activity by reducing the extent of reduction and carburization of the iron.[8,9] Studies led by Sasol have shown supported Fe catalysts have poor reaction rates and selectivities, compared to unsupported Fe catalysts, due to promoters forming chemical bonds with the support.[4] Therefore, success of supported Fe catalysts may depend on discovery of a preparation technique that weakens these chemical bonds. Since supported iron catalysts have not been extensively studied, the possibility exists that additional research could allow preparation of supported catalysts with improved activity and selectivity properties in addition to good attrition resistance.

A few published studies on supported Fe are available. They have concluded that aqueous impregnation yields strong interactions between iron and potassium oxides and the support, leading to low reducibility of iron or poor iron-promoter contact.[1,10] Xu and Bartholomew[6] attributed low reducibility of supported catalysts to ineffective preparation methods. In their study, they prepared a silica-supported catalyst (10%Fe/1%Pt/0.2%K/SiO_2) using a non-aqueous evaporative impregnation method. They even removed the water molecules of hydration by bubbling He through the nitrate salt at 80°C. The group also prepared a catalyst without K and another without K or Pt. The three resulting catalysts had high extent of reduction (60–80%) at 300°C in H_2, moderately high dispersion (5–16%), and moderate FTS activity, although the methane selectivity was still high (6–10%).

Although both aqueous and non-aqueous supported Fe catalysts have been prepared, no studies were identified that directly compared aqueous and non-aqueous preparation methods.

Other researchers have explored promotion of supported Fe catalysts. The two promoters which have been used in preparation of commercial unsupported Fe FT catalyst are potassium (K) and copper (Cu). Because CO and H_2 can both be reducing agents, redox properties of the catalyst during FTS are crucial. The addition of K on Fe-

based catalysts affects the catalytic activity for both Fischer-Tropsch Synthesis and the concurrent water-gas shift reaction.[11,12] The K also affects methane, olefin, and higher hydrocarbon selectivity.[12] Davis[11] investigated the effect of K at different conversions. Much higher CO conversions were obtained on 0.02 K/Fe atomic ratio catalysts than K-free catalysts. A K content of 0.04 K/Fe atomic ratio did not exhibit an increase in FTS activity. K loadings of 4 atomic% may appreciably cover the active sites for FTS, while K loadings above 4 atomic% begin to increase carbon deposition, blocking the surface sites and leading to further decline in activity. Thus, the level of promoter loading appears to make a critical difference.

Success of a preparation method also depends on the timing and relative order in which these promoters are impregnated onto the support. Bukur et al.[1] studied supported Fe catalysts on alumina (Al_2O_3) and silica (SiO_2) which were prepared by co-impregnation of ferric nitrate, copper nitrate, and potassium bicarbonate in successive steps to desired levels. They compared the performance of these two catalysts to the performance of two unsupported, precipitated catalysts prepared similarly. Bukur et al. estimated the extent of reduction from Fe_2O_3 to metallic Fe as 19–26% at 400℃ for both their alumina-supported and silica-supported Fe/Cu/K catalysts. Their silica-supported catalyst, however, was only one third as active as their most active precipitated Fe/Cu/K/SiO_2 catalyst when compared per gram catalyst (100 vs. 269 mmol$(CO+H_2)/g_{cat}$/MPa/h at 260℃) and their alumina-supported catalyst was only one fifth as active (i.e., about half as active as the silica-supported catalyst). The methane selectivity of the alumina-supported catalyst was comparable to the unsupported catalysts (3–4 mol%, carbon atom basis), while the methane selectivity of the silica-supported catalyst was higher (6–7 mol%, carbon atom basis).

O'Brien et al.[2] used a different impregnation method for preparing supported Fe catalysts. Ferric nitrate, copper nitrate, and potassium nitrate were melted at 70℃ and slowly added to silica, alumina, magnesium silicate, or magnesium aluminate supports. The performance of these supported catalysts was compared with an Fe/Cu/K/SiO_2 precipitated catalyst. The best supported catalyst produced in the study was only three-fourths as productive as the unsupported catalyst and again displayed higher selectivity to methane. O'Brien et al. did not report extent of reduction and dispersion for their catalysts.

Supported catalysts are one of the viable catalysts for use in SBCR's. The lack of previous work on supported Fe FT catalysts leaves gaps in the understanding the literature can provide. Although many preparation techniques have been used, the reported data lack enough consistency to isolate the effect of specific preparation variables. Determining a single preparation method's influence on the properties of a catalyst requires greater consistency. This study has examined four important variables in the preparation of supported Fe catalysts and held all other variables constant to

systematically investigate each variable's effect. The goal was to gain deeper insights into these preparation methods as a step toward designing a preparation method capable of producing catalysts with both attrition resistance adequate for use in SBCR's and high activity characteristic of precipitated catalysts. A series of K-promoted Fe catalysts supported on alumina (Al_2O_3) were prepared to examine the effect of the following *variables*: (1) impregnation method (aqueous incipient wetness or non-aqueous slurry), (2) Fe loading level, (3) K loading level, and (4) timing of impregnation (sequential impregnation or co-impregnation of K and Fe, and with or without direct K promotion of the support).

2. Experimental

2.1. Catalyst preparation

2.1.1. General preparation description

The six catalysts examined in this paper (all Fe/Cu/K/Al_2O_3) are identified as K1–K6. The timing and specific procedure for loading these metals was distinct for each of these six catalysts. These six combinations of procedures were carefully chosen to yield the most information and data about the effects of each preparation variable. Table 1 catalogs the values of each of the 4 preparation variables for the six catalysts.

Table 1. Preparation variable values for each of the six studied catalysts

	Variable 1		Variable 2	Variable 3	Variable 4
Catalyst	**Solvent**	**Deposition Method**	**Fe Loading (wt%)**	**K Loading**	**Timing of Impregnation**
K1	NA[1]	SI[3]	20	4K/100Fe	Sequential impregnation
K2	NA	SI	**40**	4K/100Fe	Sequential impregnation
K3	A[2]	IWI[4]	20	4K/100Fe	Sequential impregnation
K4	A	IWI	20	**8K/100Fe**	Sequential impregnation
K5	A	IWI	20	4K/100Fe	**Co-impregnation**
K6	A	IWI	20	4K/100Fe[5]	**K directly on support plus sequential impregnation**

[1]NA = Non-aqueous
[2]A = Aqueous
[3]SI = Slurry Impregnation (50 vol% acetone, 50 vol% isopropanol)
[4]IWI = Incipient Wetness Impregnation (aqueous)
[5]Plus 0.2 wt% K (per mass of support) added directly onto the support

The full preparation method of each catalyst is only different from the preparation of one other catalyst by a single method. All catalysts were supported on a commercial St. Gobein alumina that was sieved to 30–60 mesh (250-595 μm). Prior to any metal loading, this blank support was calcined in dry air at 700°C for 4 h to remove hydroxyl groups. The metal precursors were iron (III) nitrate nonahydrate (Sigma Aldrich, reagent grade, 98 wt%), copper (II) nitrate hydrate (Sigma Aldrich, reagent grade, 98 wt%), and potassium bicarbonate (Sigma Aldrich, reagent grade, 100 wt% dry basis). The six catalysts were impregnated with Fe, Cu, and K metals in several steps as described below. All of the supported catalysts were also calcined in dry air after each metal impregnation step for 16 h at 300°C.

2.1.2. Aqueous Incipient Wetness or Non-aqueous Slurry Impregnation

The catalysts were impregnated by one of two methods: aqueous (A) incipient wetness impregnation (IWI) or non-aqueous (NA) slurry impregnation (SI). For the aqueous method, the support was impregnated with enough aqueous solution containing the desired amount of iron nitrate and copper nitrate to just fill the pores (10 wt% Fe per loading step). The water was then slowly evaporated over 12 h at 80°C to leave only the precursors and the support.

For the non-aqueous impregnation method, an equivolume mixture of acetone and isopropanol was chosen as the solvent. Once the appropriate amount of precursor was added, the solution was mixed for 12 h at atmospheric pressure in a Yamato RE800 rotary evaporator turning at 30 rpm. Next, the solvent was evaporated over 12 h at a pressure of 70 mm Hg absolute, while still rotating at 30 rpm.

2.1.3. Iron Loading Level

Most preparation methods included 20 wt% Fe, but one catalyst (K2) was loaded to 40 wt% Fe. Fe and Cu salts were always added simultaneously in 10 wt% Fe steps at the same relative Cu atomic ratio (7.5 Cu/100 Fe). Therefore, Fe and Cu were loaded onto K2 in four separate steps, while all other catalysts had two Fe and Cu loading steps. Each loading step was always followed by calcination.

2.1.4. Potassium loading level

Except for catalyst K5, K was added in steps separate from the Fe and Cu addition. For most of the catalysts, K was added in the atomic proportion of 4 K/100 Fe. For K4, the potassium loading was doubled to 8 K/100 Fe. K6 also included additional K promoter loaded directly on the alumina support, which will be described in detail in section 2.1.5.

2.1.5. Timing of Impregnation

All catalysts, except K5, were prepared by first loading all Fe and Cu together, 10 wt% Fe at a time, and then loading all K in a separate last step. Loading K in a separate step this way is called "sequential impregnation." For K5, all of the salts, including K, were added simultaneously in each step, which is called "co-impregnation." Co-impregnation was only examined for aqueous incipient wetness impregnation because the potassium bicarbonate is not soluble in the non-aqueous solvent.

For the final catalyst, K6, 0.2 wt% potassium (per g support) was added directly onto the support by aqueous incipient wetness impregnation prior to any impregnation of Cu or Fe.

2.2. Catalyst characterization

2.2.1. Nitrogen adsorption/desorption

Brunauer, Emmett, Teller (BET) specific surface area and pore volume and pore size distribution (PSD) were calculated from nitrogen physisorption isotherms measured using a Micromeritics TriStar 3000 instrument. Average pore diameter (d_{pore}) and PSD for each catalyst were calculated using a new slab pore model and method proposed by Huang et al.[13] and modified to fit a log-normal PSD.[14] The samples (0.3 g) were degassed at 120℃ for 12 h before measurement.

2.2.2. X-ray diffraction

To estimate crystallite diameters, X-ray diffraction (XRD) patterns were collected for all the catalysts using a PANalytical X'Pert Pro diffractometer with a Cu source and a Ge monochromator tuned to the Cu-Kα1 wavelength (λ = 1.54 A°). Samples were scanned from 10 to 90° using a step size of 0.016° and a step time of 350 s. Diffraction patterns were compared to standard patterns in the International Centre for Diffraction Data (ICDD) database. The average Fe_3O_4 and Fe crystallite sizes were calculated from the Scherrer equation using the Fe_3O_4 and Fe peaks located at 2θ = 37.3° and 44.9°, respectively. Prior to XRD analysis, all samples were reduced as they would be prior to reaction (as described in Section 2.3), and then carefully passivated by first exposing each to flowing air in helium (<1 mol%) at room temperature, followed by gradually increasing concentrations of air in helium (He) while monitoring the temperature of the catalyst bed.

2.2.3. Temperature-programmed reduction (TPR)

TPR experiments were performed in a Mettler Toledo themogravimetric analyzer/differential scanning calorimeter (TGA/DSC) equipped with an automated GC 200 gas controller to determine catalyst reducibility. Calcined samples (10–20 mg) were exposed to a reducing gas mixture of 10 mol% H_2 (H_2-TPR) or 10% syngas

(H_2:CO = 1) in He (syngas-TPR), while the temperature was increased at 3 ℃/min from ambient (~25 ℃) to 700 ℃. The feed gases for the reducing mixture consisted of pure H_2 (Airgas, 99.95 mol%) and pure He (Airgas, 99.995 mol%). In order to deconvolute the weight loss due to release of strongly absorbed water, another set of TGA experiments were performed on the calcined catalysts using the same temperature profile with time, but under pure He flow. The weight loss due to water desorption was subtracted from the total weight loss of the corresponding TPR.

2.2.4. Oxygen titration

Oxygen titration experiments were performed using the equipment described in Section 2.2.3 to determine the extent of reduction (EOR) to Fe metal following reduction. The catalyst samples (10–20 mg) were reduced in situ under flowing hydrogen for 16 h at 280 ℃. They were then flushed in flowing He at 270 ℃ and during subsequent heating to 400 ℃. 10 mol% O_2 in He was introduced through the catalyst bed at 400 ℃ and the amount of oxygen consumed by the sample was calculated from the increased weight. The extent of reduction was calculated assuming that Fe in metallic form was oxidized to Fe_2O_3. Full oxidation of Cu to CuO was also assumed.

2.2.5. CO temperature-programmed desorption (CO-TPD)

CO-TPD experiments were performed to determine CO chemisorption site density. The calcined samples (0.35 g) were reduced in a quartz reactor heated by an electronic furnace in flowing 50 mol% H_2/He at 280 ℃, then purged in He at 260 ℃, subsequently cooled to 150 ℃ for CO adsorption (30 mL/min of 10 mol% CO in He for 1 h), and purged again in He to ambient temperature. Then, CO was desorbed at a heating rate of 20 ℃/min. The CO desorption rate was monitored using Pfeiffer Vacuum ThermoStar mass spectrometer.

2.3. Activity and selectivity measurements

Fischer-Tropsch synthesis (FTS) was conducted in a fixed-bed reactor (stainless steel, 3/8 inch OD) described previously.[15] Each sample (0.25 g, 250–590 μm) was diluted with 1 g quartz sand or silicon carbide to approach isothermal conditions in the catalytic zone.

Before FTS, the samples were reduced in situ at 280–320 ℃ in 10 mol% H_2 in He for 10 h, followed by pure H_2 for 6 h. After cooling to 180 ℃, the system was then pressurized to 2.1 MPa in a syngas of 63 mol% H_2 plus CO in He with H_2:CO = 1. Three calibrated Brooks (model number 5850) mass flow controllers were used to produce the reactant mixture from three feed gas cylinders (Airgas, 99.95 mol% H_2; Airgas, 88.2 mol% CO with 11.8 mol% Ar as an internal standard; and Airgas, 99.995 mol% He). The catalysts were activated at 280 ℃ for 48-90 h with a target CO conversion level of ~50% during

this carburization period. Activity and stability data were then obtained over the next 200–700 h as reaction temperatures were varied from 220℃ to 260℃.

After leaving the reactor, the exit gas and liquid effluent passed through a hot trap (90℃) and a cold trap (0℃) to respectively collect heavy hydrocarbon waxes and liquid products. The effluent gaseous product was analyzed using an HP5890 gas chromatograph equipped with a thermal conductivity detector and 60/80 carboxen-1000 column to analyze the carbon containing reactants and products up to C_2. CO conversion and selectivities were determined from the calibrated GC analysis, with aid of the Ar internal standard (premixed with the CO reactant).

3. Results

3.1. Physical properties

3.1.1. Nitrogen adsorption/desorption

Results from the nitrogen physisorption analysis, including specific surface area (SA), pore volume (V_{pore}), and average pore diameter (d_{pore}) for the calcined samples, are summarized in Table 2. The surface areas of the calcined catalysts were 152–169 m^2/g. Pore volumes were 0.45–0.54 cm^3/g, and average pore diameters were 15.9–17.4 nm. Compared to the fresh St. Gobein alumina support, these values represent a decrease after impregnation and calcination on average of 24%, 23%, and 9% for SA, V_{pore}, and d_{pore} respectively.

Table 2. Surface area, pore volume, and average pore diameter of St. Gobein support and six catalysts of this study

Catalyst	BET surface area (m^2/g)	Pore volume (cm^3/g)	Average pore diameter (nm)
St Gobein	216	0.65	18.1
K1	167	0.54	17.4
K2	152	0.45	16.4
K3	167	0.51	15.9
K4	162	0.49	15.9
K5	164	0.52	15.9
K6	169	0.51	16.9

At equivalent Fe loadings, the non-aqueous catalyst has a slightly larger pore volume than the aqueous catalyst (0.54 cm^3/g for K1 and 0.51 cm^3/g for K3). Doubling the Fe loading decreases the pore volume by 17% (0.45 cm^3/g for K2).

Fig. 1 shows the pore size distributions for all six catalysts. All of the aqueous catalysts (K3 to K6) exhibit broad bimodal distributions, with a large initial peak at about 7 nm and a second peak at about 15 nm. This first peak is smallest for K5 and especially large for K4 and K6 (the two more potassium-rich catalysts). The two non-aqueous catalysts (K1 and K2) appear to have simple, Gaussian-like, unimodal distributions about a peak at 15 nm. However, closer examination of K1 shows that a smaller peak appears at about 7 nm, precisely the same pore size as the first peak in the aqueous catalysts. This first peak disappears for the higher Fe loading (K2).

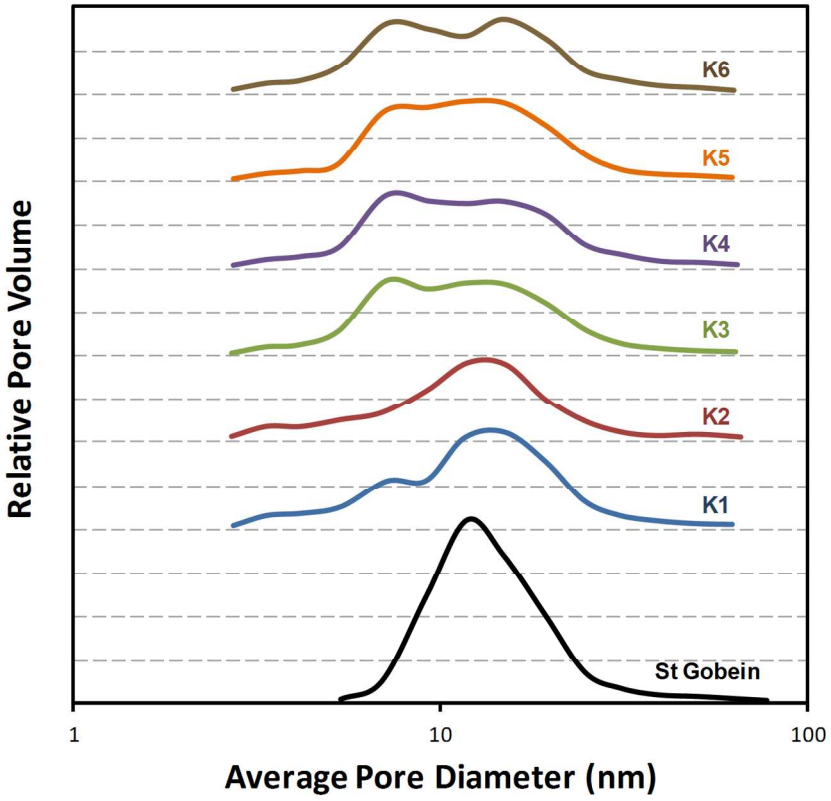

Fig. 1. Pore size distributions

3.1.2. X-ray diffraction

X-ray diffraction patterns of all six catalysts after reduction at 280℃ and passivation confirm the presence of γ-Al_2O_3 with α-Fe^0 and/or Fe_3O_4, except in the case of K6. The crystallite sizes for Fe_3O_4 and Fe^0 are given in Table 3. The Fe peaks for K6 were undetectable due possibly to crystallite sizes below the detection limit (~3 nm) or due to overlap with alumina.

Table 3. Fe^0 and Fe_3O_4 particle sizes estimated from XRD.

Catalyst	XRD	
	Fe_3O_4 particle size (nm)	Fe^0 particle size (nm)
K1		5.6
K2	6.4	11.6
K3	6.4	4.9
K4		8.6
K5	7.3	
K6	No Fe detected	

Fig. 2 shows the XRD patterns for all six catalysts. Overlapping alumina peaks dwarf the Fe^0 peak for all catalysts with 20 wt% Fe (K1 and K3 through K5). In contrast, the 40 wt% Fe catalyst, K2, has a large Fe^0 peak beside an alumina peak, which is visible as a shoulder to the right.

As shown in Fig. 2, the first five prepared catalysts displayed Fe^0 peaks. Table 3 shows that doubling the Fe loading doubles the Fe^0 crystallite size (11.6 nm for K2 compared to 5.6 nm for K1). At equivalent Fe and K loading, the aqueous catalyst (K3) has a slightly smaller Fe^0 crystallite size than the non-aqueous catalyst (K1) (4.9 vs. 5.6 nm respectively). All else being equal, doubling K loading increases the Fe^0 size by 75% (K4 vs. K3). Dry et al.[16] similarly found that K promotion increases the crystallite size of Fe metal. However, when additional potassium is impregnated directly onto the support as in K6, the opposite effect is observed. The increased basicity of the support likely provides a more favorable surface interaction, which leads to higher dispersion and apparently, to crystallite sizes below the XRD detection limit.

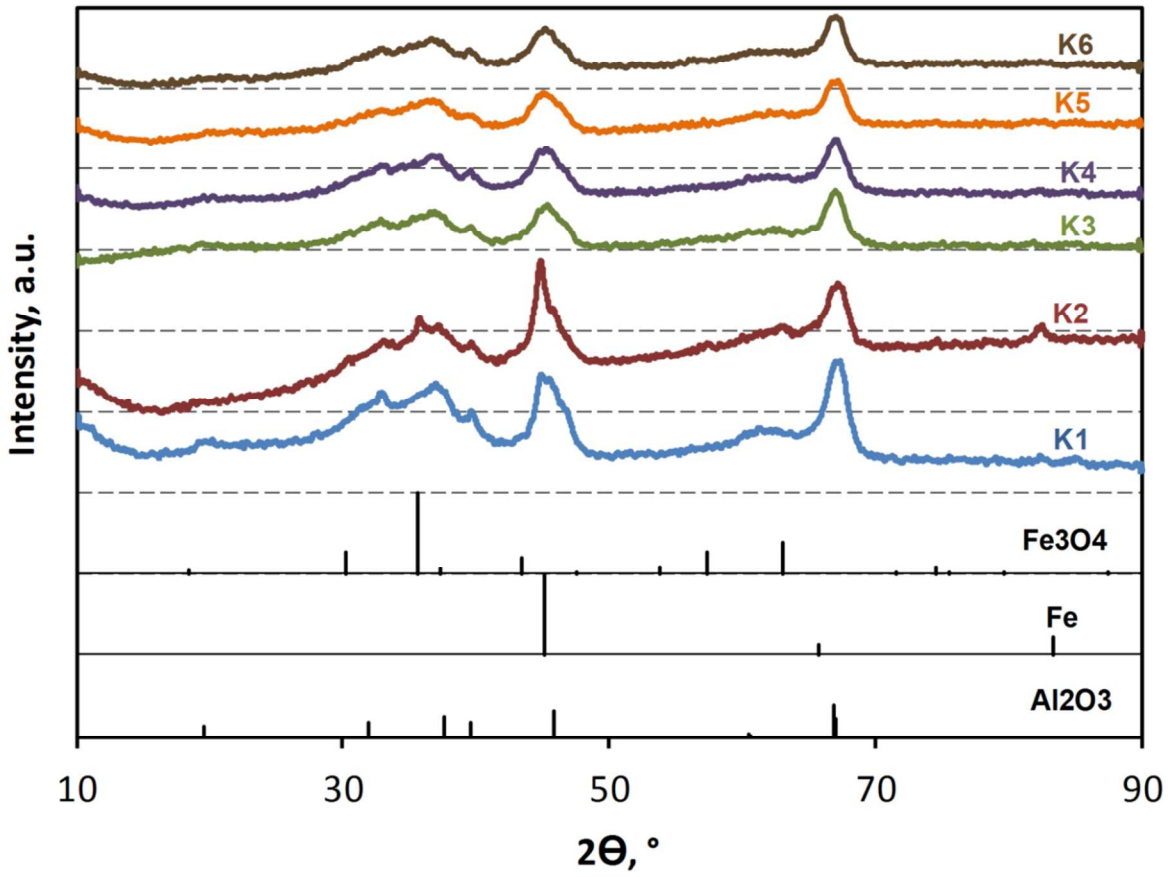

Fig. 2. X-ray diffraction patterns of passivated reduced catalysts with standards for γ-Al_2O_3, α-Fe, and Fe_3O_4.

3.2. Catalyst reducibility

3.2.1. H_2-TPR

H_2-TPR was used to investigate the effect of preparation variables on the reduction behavior of the catalysts. As shown in Fig. 3, the reduction of all six catalysts occurred in three stages with temperature ranges of 205-240°C, 310-390°C, and 470-630°C, respectively for the first, second, and third stage. The first stage is reduction from Fe_2O_3 to intermediate Fe_3O_4 and/or FeO and appears to contain two peaks, with the less intense peak generally appearing as a low temperature shoulder in Fig. 3. Catalysts K2 and K5 have two distinct peaks in this first stage, but the rest of the catalysts have shoulders centered at a temperature of ~205℃. This shoulder may be assigned to the reduction of CuO to Cu and/or Fe_2O_3 to Fe_3O_4. The second stage is an intermediate peak associated with further reduction to Fe metal. The third stage, which occurs at high temperatures, could be due to reduction of an iron-support compound, such as iron aluminate, that is too amorphous to be detected by XRD.

The highest peak on all catalysts occurs during the first stage of reduction and is relatively sharp. In contrast, the second stage, with its associated peak, is much broader, indicating that the second stage is slower.

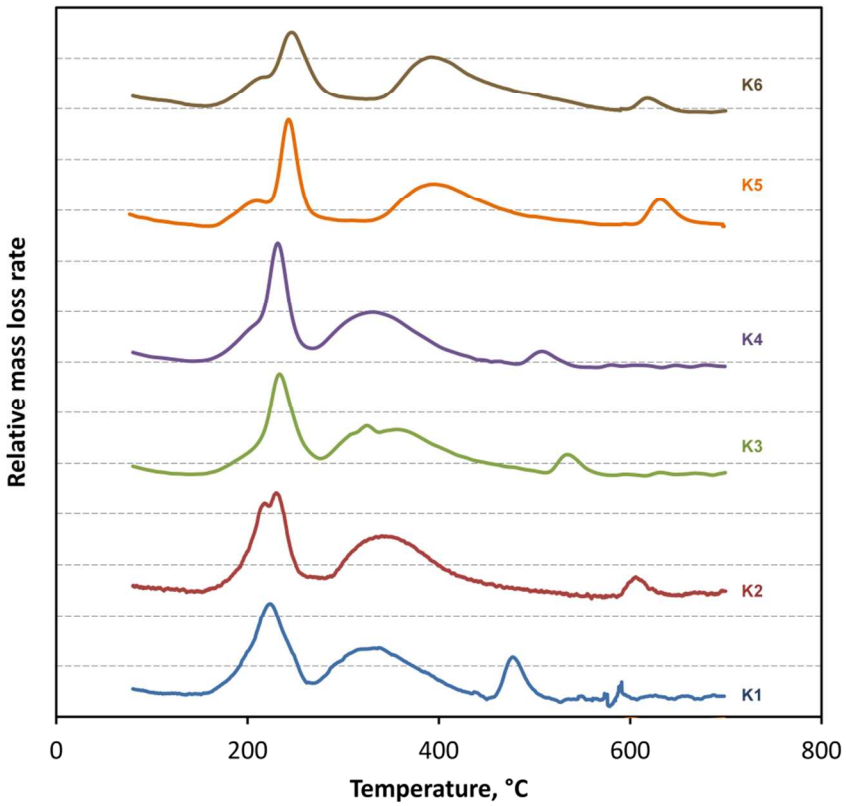

Fig. 3. Temperature-programmed reduction results

The extent of reduction for each TPR peak, reported in Table 4, was calculated by dividing the measured weight loss by the theoretical weight loss corresponding to each transition from Fe_2O_3 to Fe, including the complete reduction of CuO to Cu. The extents of reduction for the first stage (from ~205℃ to 240℃) range from 20.9 to 41.0%. These values are considerably higher than the theoretical value shown in Table 5 for reduction of Fe_2O_3 to Fe_3O_4 including CuO to Cu (14.8% extent of reduction), but closer to the theoretical value for the reduction of Fe_2O_3 to FeO (36.1% extent of reduction). This suggests that the intermediate phase in the reduction of Fe_2O_3 to Fe is likely FeO, rather than Fe_3O_4. This observation is consistent with Zhang et al.,[17] who reported that FeO, not Fe_3O_4, is the intermediate for supported Fe catalysts. As reported in Table 4, the extents of reduction for the second stage (33.5–48.8%), which is FeO to Fe metal, are less than the theoretical value (63.9%), indicating that some FeO remains in each of the six catalysts.

Table 4. Actual Extent of Reduction after TPR

Catalyst	Extent of reduction (%)	
	First stage	Second stage
K1	31.4	39.6
K2	20.9	38.5
K3	38.0	42.6
K4	40.7	33.5
K5	37.8	48.8
K6	41.0	47.8

Table 5. Theoretical Extent of Reduction

	Theoretical Extent of Reduction
Fe_2O_3 -> Fe_3O_4	14.8%
Fe_2O_3 -> FeO	36.1%
FeO -> Fe	63.9%

The highest peak for the non-aqueous catalysts (K1 and K2) occurs at lower temperatures than the four aqueous catalysts (~220℃ vs 230–245℃). However, as mentioned previously, a low temperature shoulder or peak occurs around 205℃ for all of the catalysts. K1 and K2 also have the smallest extents of reduction for both the first and second stages. K2 has an even smaller extent of reduction than K1, indicating that the additional 20 wt% Fe relative to K1 is only partially reducible. For K3 and K4, the temperatures where the highest peaks occur in the first two reduction stages are very comparable (~230℃ and 330℃, respectively). However, both of these peaks for K5 and K6 have shifted to much higher temperatures, to ~245℃ for the first stage and to ~400℃ (70℃ higher) for the second. This shift to higher temperatures indicates that K5 and K6 are more difficult to reduce than the other four catalysts.

3.2.2. Oxygen titration

The extent of reduction for the six catalysts calculated after oxygen titration at 400℃ (preceded by hydrogen reduction at 280°C) ranged from 25–44%, as shown in Table 6. The non-aqueous catalysts (K1 and K2) again have lower EOR than the aqueous catalysts (K3–K6): 25–30% vs. 38–44%. The catalyst with 40 wt% Fe loading (K2) has a lower EOR (and is more oxidized) than 20 wt% Fe (K1), despite having larger metallic

Fe crystallites (shown in Table 3). Co-impregnation (K5) results in the lowest EOR among the aqueous catalysts.

The catalysts with higher K loadings, whether added during the last stage of catalyst preparation (K4) or added to the support (K6), retain the highest extent of reduction (42–44%) following oxygen titration.

Table 6. Extent of Reduction Following Oxygen Titration at 400℃

Catalyst	EOR
K1	30.0
K2	25.0
K3	40.5
K4	44.3
K5	38.4
K6	42.4

3.3. Catalyst carbiding

3.3.1. Syngas-TPR

To evaluate the reduction/carburization behavior of the catalysts, syngas-TPR's were performed on the calcined catalysts. Fig. 4 shows the results of these syngas-TPR profiles for the six catalysts up to 350℃, the range over which the reduction/carburization of the catalysts are performed. The observed weight losses under a H_2/CO atmosphere are a combination of several competing reactions including: (1) reduction of Fe_2O_3 to lower iron oxides or iron metal (the first two peaks, 150-200℃) and (2) carbiding of the iron oxides or iron metal to iron carbides (the last peak, 280-310°C). The two step reduction of Fe_2O_3 to lower iron oxides or iron metal and its carbide occur at lower temperatures for the non-aqueous catalysts, K1 and K2. K2, with 40 wt% Fe, reduces at lower temperatures compared to K1 with 20 wt% Fe, but the reduction peak area for K2 is nearly the same as K1, which indicates a lower extent of reduction, as previously observed during the H_2 TPR. Interestingly, increasing the potassium loading in the case of K4 compared with K3 appears to facilitate easier reduction and carbiding. Co-impregnation of iron and potassium in catalyst K5, intended to produce better contact between them, results in lower reduction temperatures for the first two peaks; however, the carburization temperature does not change significantly and remains ~305℃.

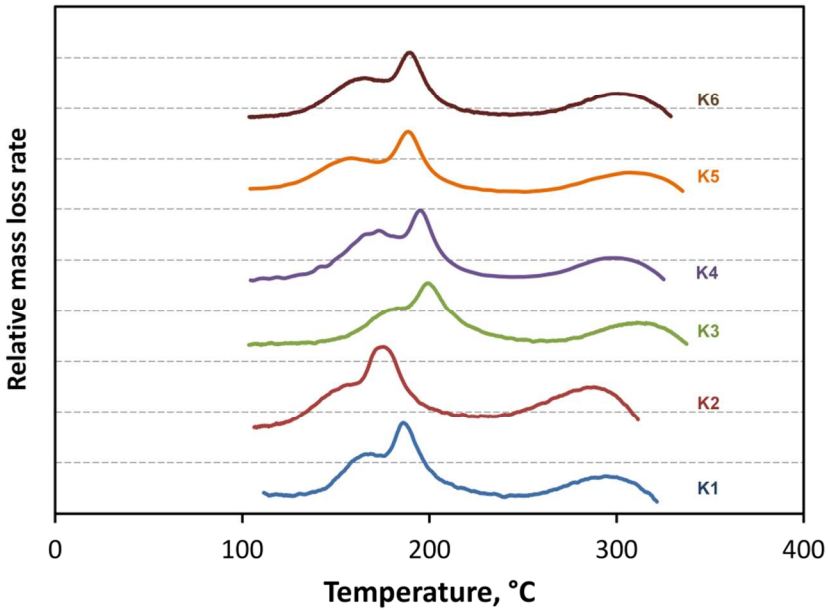

Fig. 4. Syngas-TPR profile of the alumina supported iron catalysts up to 350 ℃

3.3.2. CO-TPD

CO adsorption and dissociation on the iron surface are key elementary steps in FTS.[18] To study the effects of the various preparation variables on CO adsorption, desorption, and dissociation, the amount of CO and CO_2 evolved during CO-TPD were measured after pre-adsorption of CO, as shown in Figs. 5 and 6, respectively. Mass spectroscopy measurements indicate two peaks: the first peak (~220℃) is attributed to desorption of molecular CO (see Equation 1), while the second broad peak at higher temperatures (between ~450 and 650℃) is attributed to desorption of CO after recombination of dissociated carbon and oxygen on the surface (see Equation 2).

$$CO + * \leftrightarrow CO^* \quad (1)$$

$$CO^* + * \leftrightarrow C^* + O^* \quad (2)$$

In Fig. 5, the first peak is much smaller than the second peak, which shows that CO dissociates readily on the surface at an adsorption temperature of 150℃. For the aqueous catalysts (K3–K6), the second peak (recombination peak) is a wide or bimodal peak, beginning at significantly lower temperatures (428–455℃) compared to the same peak for the non-aqueous catalysts (~530℃). On the non-aqueous catalysts, in contrast, recombined CO elutes in a single peak at ~600℃. This second peak ends at ~650℃ for all six catalysts.

Comparing Fig. 6 with Fig. 5, the CO_2 desorption patterns are qualitatively quite different, especially for the aqueous catalysts, where the CO_2 desorbs at up to three

different temperatures, indicating up to three different sites at which CO_2 is formed. The three peaks include a relatively large one at low temperatures (230–255 ℃) and progressively smaller peaks at higher temperatures (390–415 ℃ and 605–650 ℃).

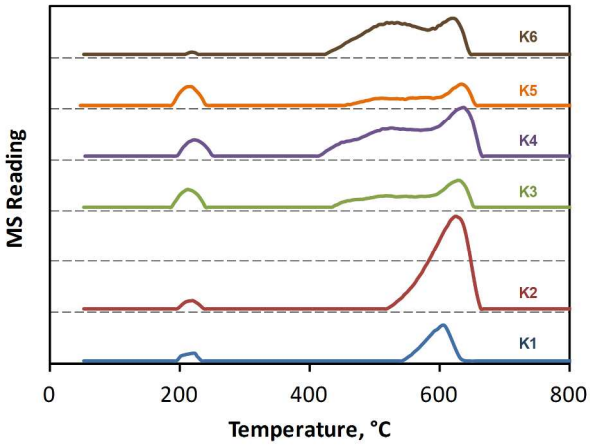

Fig. 5. CO spectra of CO-TPD after CO adsorption at 150 ℃

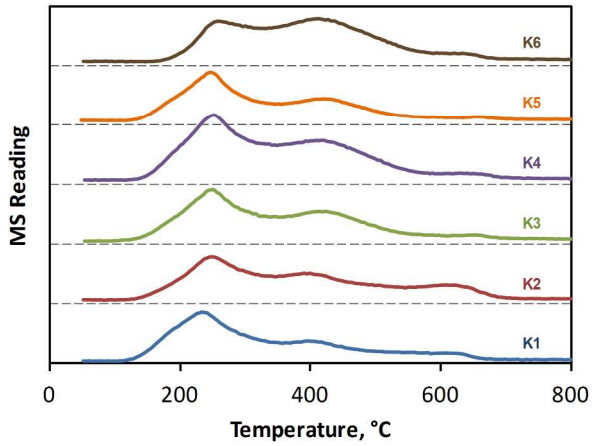

Fig. 6. CO_2 spectra of CO-TPD after CO adsorption at 150 ℃

Table 7 shows the amount of CO and CO_2 evolution and the total ($CO+CO_2$) uptake on each catalyst. As expected, the Fe loading had a large positive effect on the total ($CO+CO_2$) uptake, since additional Fe creates more adsorption sites (61.6 $\mu mol/g_{cat}$ for K1 vs 104.1 $\mu mol/g_{cat}$ for K2). However, on a per gram Fe basis, the 40 wt% Fe catalyst adsorbs less CO than the 20 wt% Fe catalyst (260 $\mu mol/g_{Fe}$ for K2 vs 308 $\mu mol/g_{Fe}$ for K1), indicating that not all of the additional Fe in K2 is available on the surface. Among the 20 wt% Fe catalysts, the two catalysts with additional potassium (K4 and K6) had the highest total ($CO+CO_2$) uptake. For K4, with twice as much potassium as K3, molecular CO desorption did not change (see the 1st peak of Fig. 5), but dissociated CO that recombined and desorbed (the 2nd peak of Fig. 5) increased from 19.5 to 47.3

$\mu mol/g_{cat}$. The additional potassium on the support of K6 decreased desorption of molecular CO to a mere 0.2 $\mu mol/g_{cat}$, but increased the total ($CO+CO_2$) uptake to 99.0 $\mu mol/g_{cat}$ compared to 80.3 $\mu mol/g_{cat}$ for K3. Co-impregnation (K5) slightly lowered ($CO+CO_2$) uptake (compared to K3). K1 and K5 have very comparable CO and CO_2 desorption behavior.

Table 7. CO uptakes on different catalysts measured by CO-TPD.

	CO signal, $\mu mol/g_{cat}$			CO_2 signal, $\mu mol/g_{cat}$	Total CO + CO_2 uptake, $\mu mol/g_{cat}$
	CO: Low temp peak	CO: High temp peaks	Total CO Peaks		
K1	1.4	12.4	13.8	47.8	61.6
K2	1.5	49.2	50.7	53.4	104.1
K3	4.4	19.5	23.9	56.5	80.3
K4	4.2	47.3	51.5	72.2	123.8
K5	4.7	12.4	17.1	43.4	60.6
K6	0.2	39.2	39.4	59.5	99.0

3.4. FTS Performance

3.4.1. Catalyst Activity and Selectivity

Activity/selectivity data were obtained at similar conversion levels of 19–28%, temperatures of 220–260℃, a total pressure of 2.2 MPa, and a constant H_2:CO feed ratio of 1.0 for the common particle size of 250 to 590 μm (30-60 mesh); therefore, measured values of activity and selectivity for the six catalysts are directly comparable. The activity for another sample of K5 with a smaller particle size of 125-177 μm (80-120 mesh) was also reported. At the operating conditions reported in Table 8, the catalysts (250 to 590 μm) have a range of reaction rates from 95 to 160 mmol ($CO+H_2$)/g_{cat}/h. Apart from the preparation variables selected and discussed in this paper, these catalysts were prepared identically. Therefore, the preparation variables examined in this paper have the largest effects on the differences in performance of the catalysts.

K5 and K6 were the most active catalysts, while K2 and K4 were the least active. Interestingly, K2 and K4 had the largest Fe loading and the largest K loading respectively. K1 and K5 had slightly better selectivity, as measured by methane production, than the other four catalysts (16–16.4% vs. 17.2–18%). Comparison of activity data from K1 (non-aqueous) with activity data from K3 (aqueous) shows that the non-aqueous slurry impregnation yields catalysts with 14% higher reaction rates (130 vs. 114 mmol ($CO+H_2$)/g_{cat}/h) and slightly lower methane selectivities (16.0% vs. 17.9%

methane). Surprisingly, doubling the Fe loading level from 20 wt% (K1) to 40 wt% (K2) decreased the reaction rate by 17%. Similarly, doubling K promotion from 4K/100Fe (K3) to 8K/100Fe (K4) lowered the reaction rate by 17%, while methane selectivity did not improve. On the other hand, direct K promotion of the support in addition to 4K/100Fe (K6) led to a significantly improved observed reaction rate (as compared with K3). However, as will be shown, direct K promotion sacrifices catalyst stability. Co-impregnation yielded a catalyst (K5) with a rate 40% higher than one prepared by sequential impregnation (K3). Co-impregnation also led to lower methane selectivity compared to sequential impregnation (16.4% compared to 17.9%).

The most active catalyst, K5, was also tested with an average particle diameter of ~150 μm (80-120 mesh). The rate increased about 24% and methane and CO_2 selectivities decreased from 16.4 to 13.2% and 41 to 33%, respectively as average catalyst particle size decreased by a factor of 3 from 420 to 150 μm. A rate increase of only 24% with a decrease in particle diameter of almost a factor of 3 indicates a minimal and decreasing pore diffusion effect. The productivity of K5 also increased about 25% to 0.75 $g_{HC}/g_{cat}/h$. The next most active supported iron catalyst (K1) was also tested at the smaller particle sizes, but no significant changes in rate or selectivity were observed, further indicating the negligible pore diffusion effect for the catalysts at the conditions of this study.

Table 8. Performance of six catalysts of this study in fixed-bed reactor tests. T = 260°C, H_2/CO = 1, P_{H2}^0 = 0.66 MPa, P_{CO}^0 = 0.66 MPa, P_{tot} = 2.2 MPa.

Catalyst ID	**K1**	**K2**	**K3**	**K4**	**K5**		**K6**
Catalyst particle size (μm)	250-595	250-595	250-595	250-595	250-595	125-177	250-595
Time on stream, h	95	126	119	119	118	60	120
Space velocity, $Nl/g_{cat}/h$	23	23	21	19	21	22	23
CO conversion, %	21	19	19	20	28	19	24
Rate[a]	130	108	114	95	160	210	149
Hydrocarbon Selectivity,[b] mol%							
CH_4	16.0	17.2	17.9	18.0	16.4	13.2	17.5
C_{3+}	76	75	73.6	73.1	74.5	81.5	73.1
CO_2 selectivity, %	39.5	42.7	40.2	43.9	40.9	33.3	42.4
Catalyst productivity[c]	0.47	0.39	0.39	0.33	0.56	0.75	0.49

[a] mmol $(CO+H_2)/g_{cat}$ /h
[b] CO_2-free basis
[c] $g_{HC}/g_{cat}/h$

3.4.2. Catalyst Stability

The reaction rate was periodically measured at 250°C over time to directly compare the stability of the catalysts. Fig. 7 shows the results of these measurements as a function of time on stream. (Data prior to ~60 h onstream during the induction period of catalyst carburization are not shown because the temperature and flow conditions were optimized for catalyst activation.) The non-aqueous catalysts, K1 and K2, are the most stable. Although K5 and K6 were initially the most active catalysts, this stability analysis conducted at 250°C reveals that neither is very stable. K6, in particular, deactivates to nearly half its initial rate in only 175 h on stream. Extrapolating this steep rate of deactivation beyond the measured 235 h on stream, K6 would have the lowest activity of the six after 300 h or less.

Initially, K5 likewise has a favorable reaction rate, but quickly deactivates. It is unclear whether the reaction rate is stabilizing for K5 after 300 h on stream. If so, K5 could possess the best combination of activity and stability of any catalyst in this study. This lab plans to conduct an additional stability study with K5 in the future, but the data available at this time are insufficient to distinguish the performance of either K1 or K5 as preferable over the other. For a comprehensive view of the quality of these six catalysts, the activity and selectivity characteristics of the catalysts shown in Table 8 should be considered in light of this stability analysis.

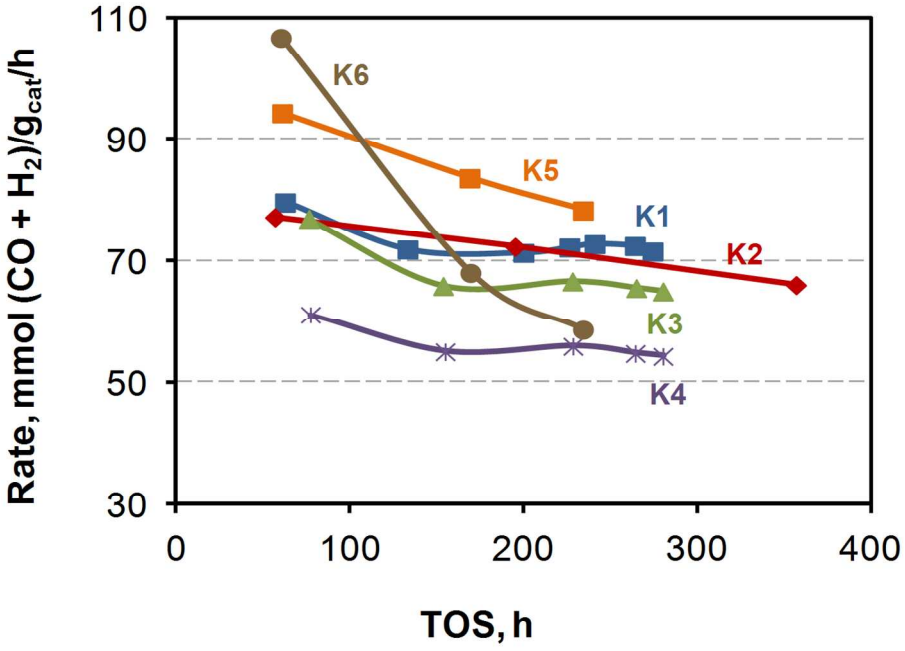

3.4.3. Activity comparison to literature

The FTS performance of the two best catalysts in this study (K1 and K5) was compared with some of the best Fe catalysts reported in the literature, including both supported and unsupported Fe catalysts. The reported data were collected at a variety of reactant concentrations and temperatures. Therefore, in order to make the comparison, a simple model was used to estimate an apparent reaction rate constant, which accounts for differences in partial pressures. A first-order reaction with respect to hydrogen and zero order in CO was assumed to calculate the apparent reaction rate constant.

A brief summary of the experimental conditions in this study follows to facilitate comparison with the literature results. The temperature and total pressure of K1 and K5 were held constant at 260°C and 2.2 MPa. These supported catalysts were sieved to a particle size of 80-120 mesh (average particle diameters of ~150 μm). For this comparison study, the reaction was performed at relatively high conversions (up to 70%) to directly compare the reaction rates and productivities with the literature reports at similar conversion levels, and the ratio of H_2/CO in the feed was about 0.67. Other catalysts reported in literature and shown in Table 9 were tested at nearly the same conditions. As is well-reported in literature,[19] higher conversion and lower H_2/CO result in slightly lower activity and lower methane selectivity. In addition, the catalysts in this paper were tested in a fixed bed reactor, while most other reported FTS rates were measured in slurry reactors. The values shown in Table 9 can be used to further understand the effects of the techniques used to prepare K1 and K5.

The catalysts reported in Table 9 are among the most competitive reported in the literature to date. Using rate per MPa for comparison removes much of the bias of differing conversions and H_2/CO ratios. Although K5 (*supported* iron) has a lower rate than the most reactive *unsupported* catalyst in Table 9, TAMU1 (152 vs 269 mmol $(CO+H_2)/g_{cat}/MPa/h$), K5 produced virtually the same rate as a commercial *unsupported* catalyst from Ruhrchemie, as reported by Bukur's group[20] (154 vs. 155 mmol $(CO+H_2)/g_{cat}/h$, respectively).

The activities of K1 and K5 are superior to any supported catalysts reported in the literature prior to publication of our recent work on Fe supported on silica doped alumina.[21] Both K1 and K5 have 17-40% higher reaction rates than the next most reactive supported catalyst (TAMU2, $40Fe/SiO_2$). Per gram Fe, the extremely high reaction rates of K1 and K5 demonstrate how effective the Fe is utilized in each catalyst (570 mmol $(CO+H_2)/g_{Fe}/MPa/h$ for K1 and 770 mmol $(CO+H_2)/g_{Fe}/MPa/h$ for K5).

Hydrocarbon selectivities (based on methane production) for K1 and K5 are less favorable than those prepared by Bukur et al. (see Table 9). The C1 selectivity of K5 on

a CO_2-free basis is higher (11.4 vs. 7%) than that of Bukur's supported catalyst (TAMU2).

This lab recently reported successful preparation of a supported Fe catalyst using a thermally stable silica-doped alumina support.[21] This catalyst yielded a methane selectivity of 9.6% at similar operating conditions (reaction T = 260 ℃, H_2/CO=0.66, and X_{CO}=72%) to TAMU2. In addition, this AlSi-supported Fe catalyst is more active than all the catalysts in Table 9.[21] More significantly for this similar AlSi-supported Fe catalyst, increasing the conversion from 23 to 72% resulted in only moderately lower activity, with the 1st order rate constant decreasing from 396 to 325 mmol $(CO+H_2)/g_{cat}$/MPa/h) and productivity decreasing from 0.72 to 0.50 g_{HC}/g_{Fe}/h. The activities of the catalysts in the present study are 1.5-3 times higher than the other supported iron catalysts reported in Table 9.

Table 9. Comparison of K1 and K5 performance with catalysts reported in the literature

	Catalyst							
	BYU[a]		TAMU1[b]	Ruhrchemie[c]	TAMU2[d]	TAMU3[e]	U. Kentucky[f]	BYU-Xu[g]
Run ID	K1	K5	Unsupp.	Unsupp.	SiO_2/ supp.	Al_2O_3/ supp.	Al_2O_3/supp.	SiO_2/supp.
Literature ref.	This study		5	20	1	1	2	3
Reactor	Fixed bed		slurry	slurry	slurry	slurry	slurry	Fixed bed
Temperature, ℃	260	260	260	260	260	260	250	265
Pressure, MPa	2.2[h]	2.2[h]	2.2	1.5	1.5	1.5	1.3	1
Inlet H_2/CO	0.67	0.68	0.68	0.67	0.67	0.67	0.7	1
Space velocity, $Nl/g_{cat}/h$	5.0	3.7	3.5	2.2	1.4	1.3	0.68	1.9
TOS, h	183	183	86		100	100	300	150
CO conversion, %	39	70	84	66			60	77
$-r_{CO}$, mmol $(CO)/g_{cat}/h$	38[i]	52[i]	76	38			18	14
k, mmol $(CO+H_2)/g_{cat}$/MPa/ h	114[j]	154[j]	269	155	101	50.7		62.1

k, mmol $(CO+H_2)/g_{Fe}$/MPa/h	570[j]	770[j]	450	290	300	150		621
H.C. selectivities, wt%[k]								
CH_4	10	11.4	3	5.3	7	3.5	5.8	6.8
C_{3+}	85.8	83.6	90.1					
$CH_4+C_2H_6$	14.2	16.4	6.3					
Catalyst productivity[l]	0.26	0.29	0.51	0.27			0.076	0.3
Catalyst productivity[m]	1.3	1.45	0.86	0.51			0.35	3

[a] 100Fe/7.5Cu/4K/400Al_2O_3.
[b] 100Fe/3Cu/4K/16SiO_2.
[c] 100Fe/5Cu/4.2K/25SiO_2.
[d] 100Fe/5Cu/6K/139SiO_2.
[e] 100Fe/5Cu/9K/139Al_2O_3.
[f] 100Fe/6Cu/8.1K/250Al_2O_3.
[g] 10%Fe/1%Pt/0.2%K/88.8%SiO_2.
[h] P_{H2}^0 = 0.66 MPa, P_{CO}^0 = 0.66 MPa, P_{tot} = 2.2 MPa
[i] average rate from inlet to the outlet of reactor
[j] an isothermal integral reactor model was used to calculate the rate constants with a rate expression of the form kP_{H2}; volume change factors of -0.44 and -0.425 were assumed for K1 and K5, respectively.
[k] CO_2 free basis.
[l] g_{HC}/g_{cat}/h.
[m] g_{HC}/g_{Fe}/h.

4. Discussion

By carefully pairing and comparing catalysts with only one dissimilar preparation variable, the direct effects of each specific preparation method on catalyst selectivity, activity, and stability can be discerned. The differences in each pair of catalysts are analyzed below and labeled by their associated preparation variable.

4.1. Choice of solvent: aqueous vs non-aqueous (K1 vs. K3)

Control of distribution of active precursors is dependent upon the impregnation method and drying step. A uniform distribution in incipient wetness impregnation is usually difficult to obtain. However, wet impregnation in a rotary evaporator greatly facilitates uniform filling of the pores with the precursor solution. Recently, Sasol showed that slurry impregnation, as in the case of the non-aqueous preparation method, leads to better dispersion compared to an incipient wetness preparation method.[22,23] Also, several papers from de Jong's group showed that improved dispersion in turn improves stability; higher dispersion introduces physical voids between active sites, thus reducing sintering.[8,24,25]

Tymowski et al.[26] conducted a set of transmission electron microscopy (TEM) tomography experiments that show water does not wet pores smaller than 50 nm, while non-aqueous solvents wet pores as small as 4 nm. This difference allows non-aqueous impregnation to disperse the active phase throughout a wider range of pore sizes, leading to improved dispersion and activity. In addition, the metal deposited in this smaller range of pores (4 nm to 50 nm) with non-aqueous solvents may strengthen the pores against collapse. This may explain why K1 has slightly larger pore volume than K3 (0.54 vs. 0.51 cm^3/g). As observed in the BET results section, K1 exhibits a muted first peak at 7 nm that corresponds to peaks in the aqueous catalysts. The non-aqueous catalyst's first peak disappearing may be due to smaller pores (5–7 nm in diameter) being filled with Fe during impregnation. This argument also explains why this first pore size distribution peak on K2 (40 wt% Fe) has disappeared altogether.

During drying of each sample after impregnation, especially the ones using an aqueous solution, capillary transport may cause the active precursor to accumulate at pore entrances, ultimately leading to a shell-type distribution of metals. Tymoski et al.[26] also hypothesized that metals could be drawn out of pores in the drying step of preparation, leading to pore plugging. Iglesia's group[27] proposed that sintering can occur via pore mouth pinching in the last stages of evaporation of the solvent during preparation. They stated that this sintering is particularly severe for solvents with high surface tensions. Therefore, the lower surface tension of the non-aqueous solvent (50 vol% acetone, 50 vol% isopropanol) may lead to better dispersion for K1 and K2 by way of less disruptive drying. (The surface tensions of acetone, isopropanol, and water at 20°C are 23.4, 23.0, and 72.8 mN/m, respectively.)

As stated in the preparation section, K1 and K2 were prepared in a rotary evaporator with non-aqueous slurry solution, while the aqueous catalysts were prepared by incipient wetness impregnation. Both the slurry impregnation and the non-aqueous solution likely contributed to improve the uniform distribution of the active precursors, consequently resulting in higher activity (130 vs. 114 mmol $(CO+H_2)/g_{cat}/h$) and better stability for K1.

4.2. Fe loading level: 20 wt% vs 40 wt% (K1 vs K2)

Bukur et al. stated that high metal loading for supported Fe catalysts is essential to achieve high reactor productivity.[1] However, pore plugging can be exacerbated by higher metal loadings. In this study, as previously mentioned, doubling the Fe loading actually decreased the reaction rate per g of catalyst by 17%. The additional Fe in K2 (20 wt% more than K1) appears to block the pores from reactants, as evidenced by a 17% lower pore volume of K2 than K1. In addition, H_2-TPR results show that the

additional Fe in K2 is harder to reduce than K1. For each support, an optimal Fe loading exists that fills the pore volume without blocking reactants from accessing the pores. This optimal loading level likely depends on the pore volume of the support used. In another paper produced by our group [19], catalysts on another support (with double the pore volume of St. Gobein alumina) exhibited improved activity with 40 wt% Fe compared to 20 wt% Fe. For the procedure used to prepare K1 and K2, a critical threshold exists somewhere below 40 wt% Fe for maximum surface area per gram Fe. Therefore, the optimal Fe loading for catalysts on the St. Gobein support must be a loading less than 40 wt%.

4.3. Potassium loading level: 4K/100Fe vs 8K/100Fe (K3 vs K4)

Generally, K promotion of FT catalysts is thought to increase activity of both FTS and the water-gas shift reaction. Davis[11] studied trends for potassium-promoted FTS at various conversion levels. He found additional K actually decreases FTS activity at low CO conversions, where K seems to act as a poison. As conversion increases, hydrogen becomes a limiting reagent and FTS begins to depend on hydrogen formed by the water-gas shift reaction. At high conversion, K slightly enhances the FTS activity. Therefore, at intermediate conversions, a K loading exists that produces a catalyst with maximum FTS activity. Specifically, Li et al.[27] observed that K addition above the amount required to create surface density of 1 atom/nm^2 does not increase reaction rate.

For this particular set of catalysts, the additional K applied to K4 appears to have surpassed the loading for maximum rate (for operation at low conversions, <28%). This explains why K4 has a lower reaction rate than K3. Alternatively, Torres Galvis et al.[24] showed that lowering the Fe carbide particle size on carbon nanofibers increased the catalytic activity. In the case of K4, doubling the K loading increased the crystallite sizes of Fe metal (8.6 vs. 4.9 nm), which may also contribute to the lower activity observed of K4 compared to K3. Surprisingly, the methane selectivity of K4 was virtually unaffected by the additional K at this level of CO conversion (20%).

4.4. Impregnation timing: sequential impregnation vs co-impregnation; direct surface promotion of the support (K3, K5, K6)

Catalyst preparation by co-impregnation (K5) produces a rate 40% larger than sequential impregnation (K3). H_2-TPR results (Fig. 3) for K5 reveal the reason for this significant difference: the profile for K5 exhibits shifts to higher temperatures for the first and second peak, by 15°C and 70°C, respectively, compared to the profile for K3. The addition of K and Fe simultaneously seems to have placed the two metals in close contact, making K5 less reducible.[11] This close contact is likely also the cause of the improved reaction rate and methane selectivity for co-impregnation (K5). This TPR

peak shift is coupled with a lower EOR than the other aqueous catalysts, likely again due to intimate contact of Fe and K.

Dry and Oosthuizen reported that K^+ ions are an effective promoter because they increase surface basicity.[16] Surface basicity improves dissociation of CO and leads to production of longer hydrocarbons. CO-TPD results demonstrate higher ($CO+CO_2$) uptake on K6 than K3 (99 vs. 80.3 $\mu mol/g_{cat}$) as surface basicity increased by loading of K on the support. Therefore, adding K on the support increased the rate by 31% (relative to K3). Unfortunately, the data presented in Fig. 4 clearly demonstrate that K6 is not a stable catalyst. During the first 200 h of testing, K6 deactivated dramatically due probably to carbon deposition on the surface of the catalyst, or possibly redistribution of the potassium.

CO-TPD showed that K4 and K6 both have significant dissociation of CO on the surface. Recently, Ribeiro et al.,[28] using in-situ TPR-extended X-ray absorption fine structure/X-ray absorption near edge spectroscopy (EXAFS/XANES), found that the rate of carburization correlates with the basicity of the alkali oxide, which is consistent with higher CO dissociation on both K4 and K6 that have higher potassium loading. Furthermore, they reported that the Hägg carbide is the most abundant iron carbide, which is consistent with our observations for K1, with the XRD reported in a previous paper.[21] Both of these potassium-rich catalysts probably deactivate due to carbon deposition brought on by basic catalyst surfaces. Addition of K on the surface of the alumina clearly exacerbated the deactivation of K6 compared to not adding it (K3).

H_2-TPR results show a shift to higher reduction temperatures for K6 compared to K3. This effect is not simply caused by additional potassium, because K4 exhibited no such change. Possibly, the peaks for K6 have shifted due to Fe or FeO interacting with the potassium-modified surface of the alumina.

5. Conclusions

The effects of the four catalyst preparation variables studied by comparing the catalyst performance of pairs of catalysts with only a single preparation variable differing between them were significant. The resulting observations are summarized below:

1. **Aqueous incipient wetness vs. non-aqueous slurry:** K1 (non-aqueous slurry) has 14% higher activity and improved stability compared to K3 (aqueous incipient wetness). Non-aqueous solvents allow for a more gentle drying process that apparently does not disturb the impregnated Fe within the pore.
2. **Fe loading level:** K1 (20 wt% Fe) has a 17% higher reaction rate than K2 (40 wt% Fe) per gram of catalyst. In this case, lower Fe loading may avoid blocking

the pores on St. Gobein alumina and so yields greater rates compared to the higher Fe loading.

3. **K loading level:** K3 (4 K/100 Fe) has a 20% higher reaction rate than K4 (8 K/100 Fe). Additional K beyond 4 K/100 Fe acts as a poison at the low conversions used in this study (<28%).
4. **Timing of impregnation:** K5 (co-impregnation) has a 40% higher rate than K3 (sequential impregnation) at 260°C. Co-impregnation of Fe and K yields a catalyst with intimate contact between Fe and K inside the catalyst pores. K6 (direct K promotion of the support) deactivates sharply in the first 200 h on stream, while K3 (no K promotion of the support) is far more stable. Direct K-promotion of the support increases the FTS reaction rate, but also appears to increase the rate of carbon deposition.

Based on these results, we predict that the optimal sequence of preparation methods (for this St. Gobein alumina support) combines non-aqueous slurry impregnation with co-impregnation of Fe and K metals, with 20 wt% Fe and 4 K/100 Fe. The optimal preparation method also does not directly promote the support with K. The optimal Fe loading could be less than or greater than 20 wt%, but an Fe loading as high as 40 wt% blocks the pores limiting reactant access to active sites. Likewise, the optimal K loading could be less than or greater than 4 K/100 Fe, but must be less than 8 K/100 Fe for low CO conversions. Since K1 and K5 had the best activity, stability, and selectivity performance of the six catalysts, perhaps a catalyst prepared by both non-aqueous slurry impregnation and co-impregnation with potassium would perform better than K1 and K5. Unfortunately, a catalyst could not be prepared with this combination of preparation variables because the potassium precursor (potassium bicarbonate) is not soluble in the non-aqueous solvent. Another potassium precursor that would allow successful combination of these two preparation methods may yield superior catalysts. Measured performance of K1 and K5 demonstrates that supported Fe catalysts can have high reaction rates and high productivity, even more promising than all of the supported iron catalysts from the literature compared in this paper.

References:

1. D. B. Bukur and C. Sivaraj, *Applied Catalysis A: General*, 2002, 231, 201-214.
2. R. J. O'Brien, L. Xu, S. Bao, A. Raje and B. H. Davis, *Applied Catalysis A: General*, 2000, 196, 173-178.
3. J. Xu, C. H. Bartholomew, J. Sudweeks and D. L. Eggett, *Topics in Catalysis*, 2003, 26, 55.
4. M. E. Dry, eds. J. R. Anderson and M. Boudart, Springer-Verlag, 1981, pp. 159-255.
5. D. B. Bukur and X. Lang, *Ind. Eng. Chem. Res.*, 1999, 38, 3270–3275.
6. J. Xu, C. H. Bartholomew, J. Sudweeks and D. L. Eggett, *Top. Catal.*, 2003, 26, 55-71.
7. R. B. Anderson, *The Fischer-Tropsch Synthesis*, Academic Press, New York, 1984.
8. H. M. T. Galvis, J. H. Bitter, C. B. Khare, M. Ruitenbeek, A. I. Dugulan and K. P. d. Jong, *Science* 2012, 335, 835-838.

9. H. Wan, B. Wu, H. Xiang and Y. Li, *ACS Catalysis*, 2011, 2, 1877-1883.
10. M. Rameswaran and C. H. Bartholomew, *J. Catal.*, 1989, 117, 218.
11. B. H. Davis, *Technology development for iron Fischer-Tropsch catalysis*, University of Kentucky, 1999.
12. W. Ma, G. Jacobs, U. M. Graham and B. H. Davis, *Topics in Catalysis*, 2013.
13. B. Huang, C. H. Bartholomew and B. F. Woodfield, *Microporous and Mesoporous Materials*, 2014, 184, 112-121.
14. C. Chu, M. Hamidy and K. Nobe, *Journal of Chemical and Engineering Data*, 1971, 16, 327–331.
15. K. M. Brunner, PhD, Brigham Young University, 2012.
16. M. E. Dry and G. J. Oosthuizen, *J. Catal.*, 1968, 11, 18-24.
17. C.-H. Zhang, Y. Yang, B.-T. Teng, T.-Z. Li, H.-Y. Zheng, H.-W. Xiang and Y.-W. Li, *Journal of Catalysis*, 2006, 237, 405–415.
18. C. H. Bartholomew and R. J. Farrauto, *Fundamentals of Inductrial Catalytic processes*, John Wiley & Sons, Second edn., 2006.
19. K. Keyvanloo, W. C. Hecker, B. F. Woodfield and C. H. Bartholomew, *Submitted to Journal of Catalysis*, 2014.
20. W. Ma, Y. Ding, V. H. C. Vazquez and D. Bukur, *App. Catal., A* 2004, 268, 99-106.
21. K. Keyvanloo, M. K. Mardkhe, T. M. Alam, C. H. Bartholomew, B. F. Woodfield and W. C. Hecker, *ACS Catalysis*, 2014.
22. P. Gibson, presented in part at the Syngas Convention, Cape Town, South Africa, 2012.
23. P. J. van Berge, J. van de Loosdrecht, E. A. Caricato, S. Barradas, B. H. Sigwebela, Assignee: Sasol Technology (Proprietary) Limited; *US Pat.,* 6 455 462 2001.
24. H. M. T. Galvis, J. H. Bitter, T. Davidian, M. Ruitenbeek, A. I. Dugulan and K. P. d. Jong, *J. Am. Chem. Soc.*, 2012, 134, 16207−16215.
25. *US Pat.,* 0259026, 2012.
26. B. D. Tymowski, Y. Liu, C. Meny, C. Lefevre, D. Begin, P. Nguyen, C. Pham, D. Edouard, F. Luck and C. Pham-Huu, *Applied Catalysis A: General*, 2012, 419-420, 31-40.
27. S. Li, S. Krishnamoorthy, A. Li, G. D. Meitzner and E. Iglesia, *Journal of Catalysis*, 2002, 206, 202-217.
28. M. C. Ribeiro, G. Jacobs, B. H. Davis, D. C. Cronauer, A. J. Kropf and C. L. Marshall, *J. Phys. Chem. C*, 2010, 114, 7895-7903.

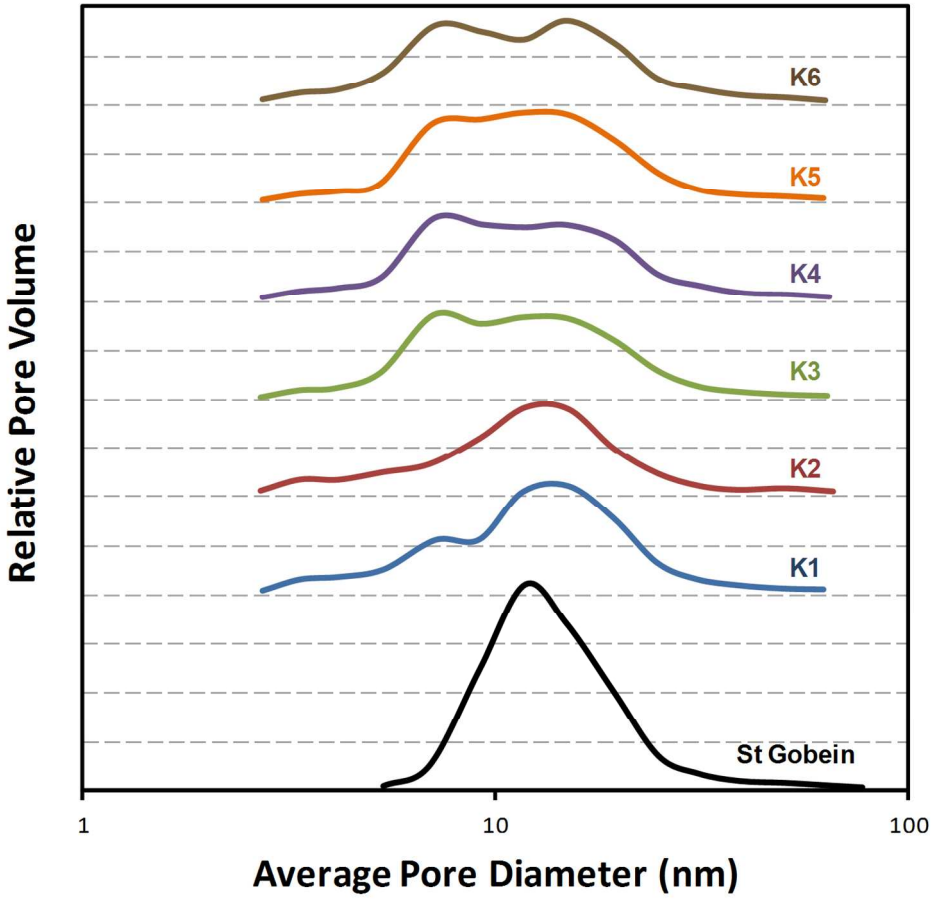

Fig. 1. Pore size distributions.
135x129mm (300 x 300 DPI)

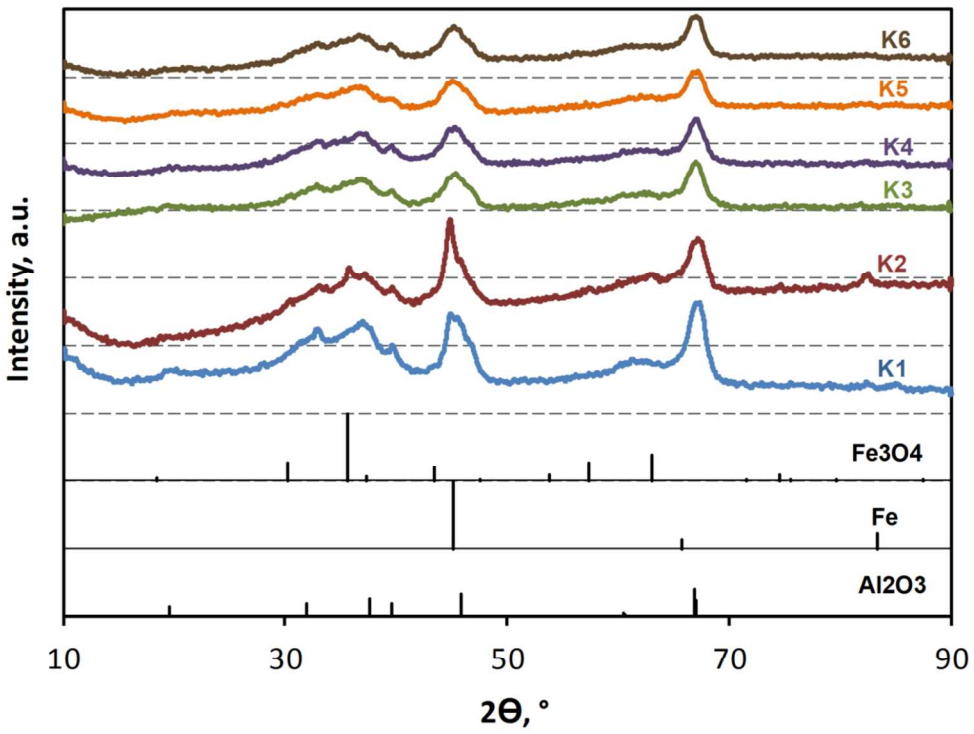

Fig. 2. X-ray diffraction patterns of passivated reduced catalysts with standards for γ-Al2O3, α-Fe, and Fe3O4.
159x122mm (220 x 220 DPI)

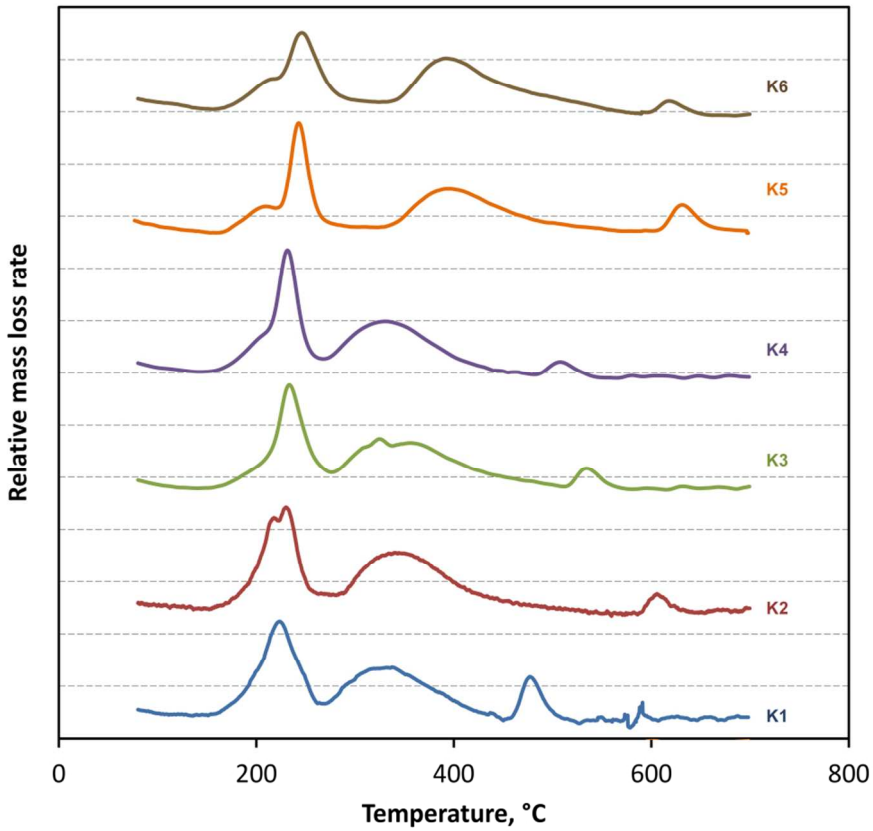

Fig. 3. Temperature-programmed reduction results.
128x110mm (220 x 220 DPI)

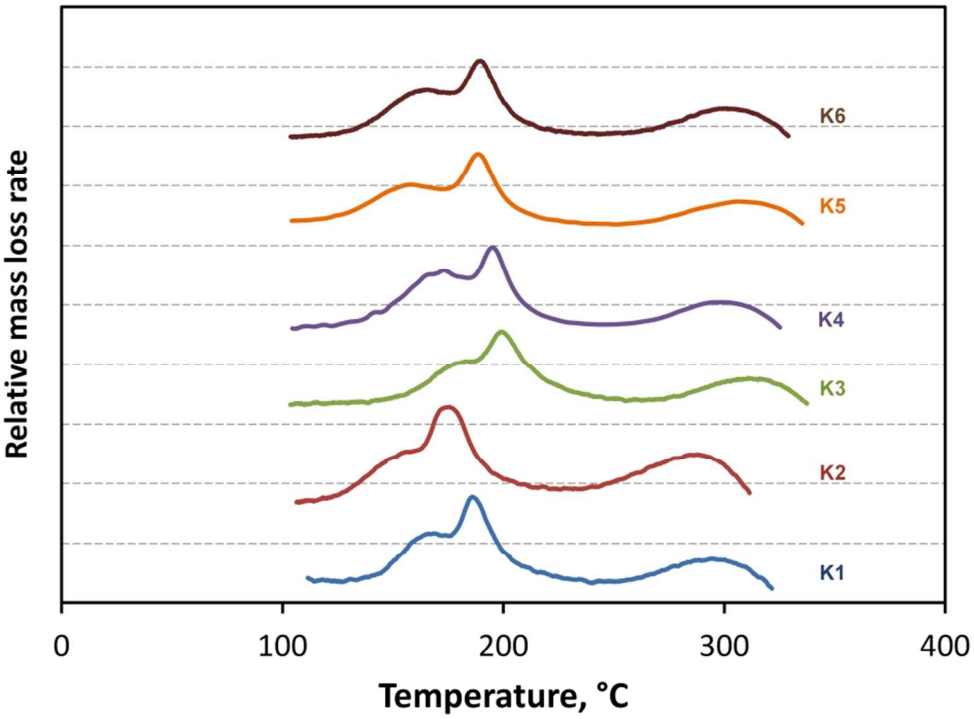

Fig. 4. Syngas-TPR profile of the alumina supported iron catalysts (a) up to 350 °C.
112x85mm (220 x 220 DPI)

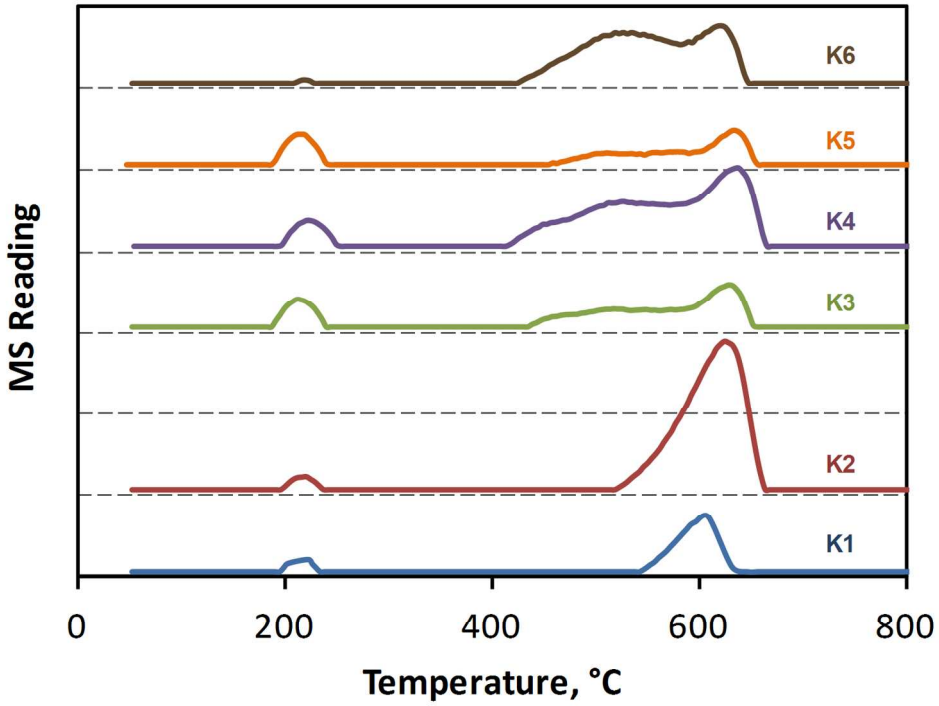

Fig. 5. CO spectra of CO-TPD after CO adsorption at 150°C
143x107mm (300 x 300 DPI)

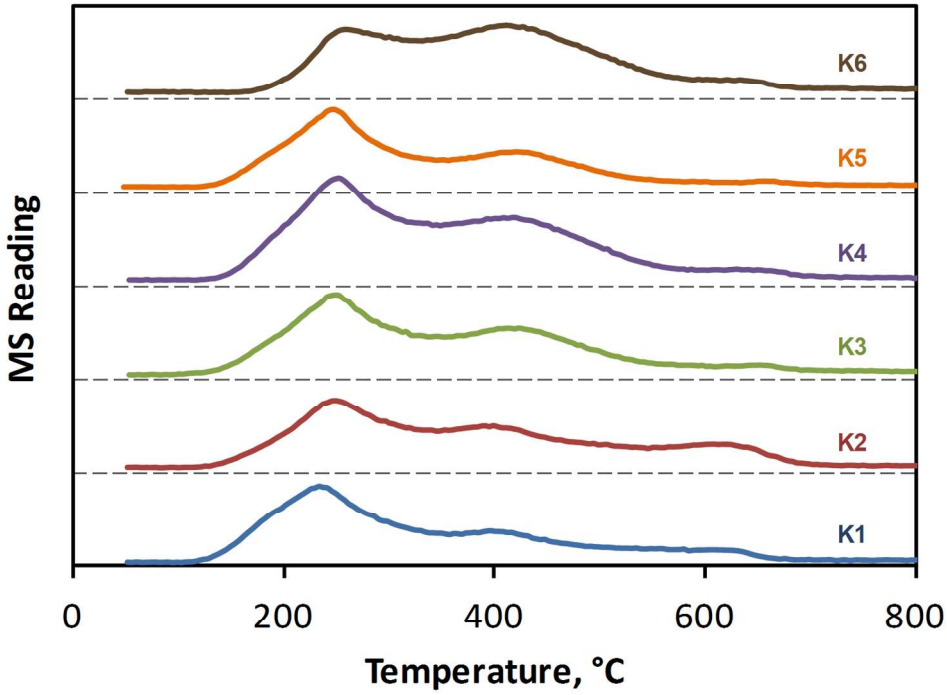

Fig. 6. CO2 spectra of CO-TPD after CO adsorption at 150°C
144x107mm (300 x 300 DPI)

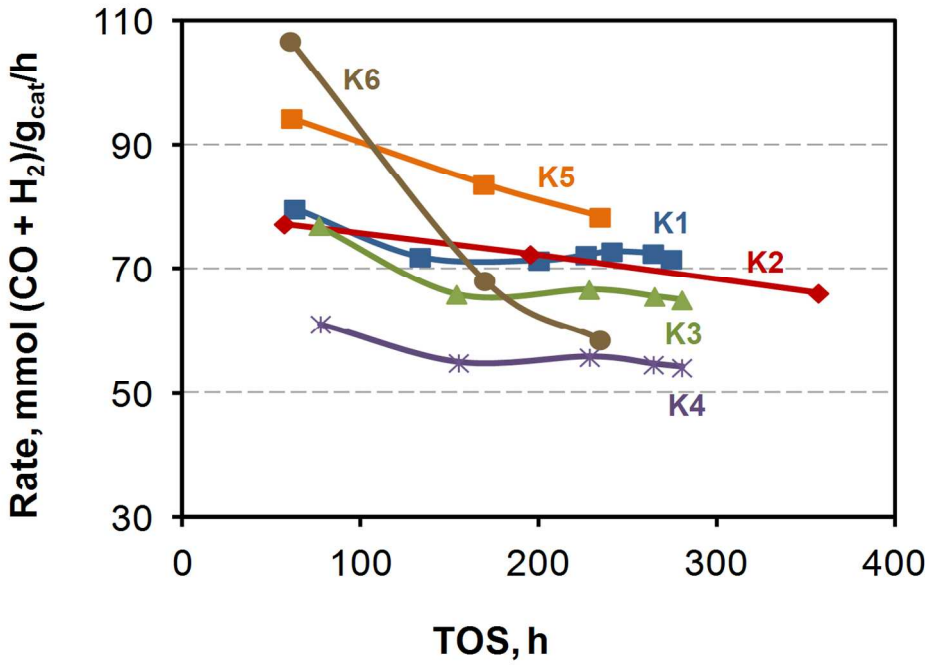

Fig. 7. Catalyst activity at 250°C vs time on stream
133x96mm (300 x 300 DPI)